Tracing Cellular Senescence in Bone: Time-Dependent Changes in Osteocyte Cytoskeleton Mechanics and Morphology

Junhan Liao [1], Domenic J. Cordova [1], James L. Kirkland [2], Kyle M. Miller [3], Maryam Tilton [1*]

[1] Walker Department of Mechanical Engineering, The University of Texas at Austin, Austin, TX, USA

[2] Center for Advanced Gerotherapeutics, Division of Endocrinology, Department of Medicine, Cedars-Sinai Medical Center, Los Angeles, CA, USA

[3] Department of Molecular Biosciences, The University of Texas at Austin, Austin, TX, USA

***Corresponding author: maryam.tilton@austin.utexas.edu**

Abstract

Aging-related bone loss significantly impacts the growing elderly population globally, leading to debilitating conditions such as osteoporosis. Senescent osteocytes play a crucial role in the aging process of bone. This longitudinal study examines the impact of continuous local and paracrine exposure to senescence-associated secretory phenotype (SASP) factors on senescence-associated biophysical and biomolecular markers in osteocytes. We found significant cytoskeletal stiffening in irradiated osteocytes, accompanied by expansion of F-actin areas and a decline in dendritic integrity. These changes, correlating with alterations in pro-inflammatory cytokine levels and osteocyte-specific gene expression, support the reliability of biophysical markers for identifying senescent osteocytes. Notably, local accumulation of SASP factors had a more pronounced impact on osteocyte properties than paracrine effects, suggesting that the interplay between local and paracrine exposure could substantially influence cellular aging. This study underscores the importance of osteocyte mechanical and morphological properties as biophysical markers of senescence, highlighting their time-dependence and differential effects of local and paracrine SASP exposure. Collectively, our investigation into biophysical senescence markers offer unique and reliable functional hallmarks for non-invasive identification of senescent osteocytes, providing insights that could inform therapeutic strategies to mitigate aging-related bone loss.

1. Introduction

Age-related bone loss impacts over 43 million Americans aged 50 and older, with a projected 47.5% increase in prevalence among those aged 65 and over [1]. This bone loss contributes to osteoporosis and fragility fractures, which remain leading causes of disability, morbidity, and mortality among the elderly. With the global demographic shift towards an aging population, where over 11,000 Americans turn 50 daily and projections indicate that by 2030, all "baby boomers" will be at least 65 years old [2–4] , the urgency to understand the degenerative mechanisms of bone loss becomes a public health priority.

Bone loss is associated with the increased accumulation of senescent cells (SnCs), including senescent osteocytes, and their senescent-associated secretory phenotypes (SASP). Indeed, most cells undergoing senescence develop SASPs that entail release of proinflammatory, proapoptotic, and pro-fibrotic factors [5]. Accumulation of SnCs can have local and systemic detrimental effects due in part to SASP factors [5,6]. To a certain extent, SnCs can be cleared naturally by innate and adaptive immune cells. However, proapoptotic SASP-expressing SnCs can induce paracrine and endocrine signals, spreading senescence at a rate exceeding immune clearance of existing or newly developed SnCs. This results in accumulation of SnCs at different pathological sites with age [7]. Specifically, SASP factors can induce senescence in normal, non-SnCs both locally and systemically [8].

SASP factors include pro-inflammatory cytokines, chemokines, growth factors, proteases, and bio-active lipids [9]. In bone, the accumulation of SnCs disrupts the balance between bone formation and resorption, driving the progression of osteoporosis and increasing the risk of fractures [10,11]. The SASP factors secreted by these cells alter the bone microenvironment, enhancing osteoclastic activity and reducing bone density.

The cytoskeleton of cells consists of actin microfilaments, intermediate filaments, and microtubules, providing mechanical support, maintaining cell shape, and playing critical roles in intracellular transport, cell division, and molecular signaling. Under mechanical stimulation, the cytoskeleton remodels, including the reorganization of stress fibers, which supports cellular functions by adapting to changes in their mechanical environment [12–14]. Osteocytes, the "superstars" in the bone microenvironment, are master regulators of bone homeostasis, being endocrine cells that regulate phosphate metabolism in organs such as the kidney and parathyroid, and most importantly, acting as strain gauges, regulating bone mechanosensation and

mechanotransduction. Specifically, the osteocyte cytoskeleton is crucial to their function, including cell-extracellular matrix (ECM) interactions via focal adhesions [15,16]. Previous studies have demonstrated that SnCs such as senescent mesenchymal stem cells (MSCs) and epithelial cells, undergo alterations in cytoskeletal architecture, potentially impairing their mechanotransduction capabilities. These cytoskeletal changes in aging osteocytes offer opportunities to investigate unique senescence-related biophysical markers, reflecting alterations in their mechanobiological functions.

Cellular senescence is characterized by essentially irreversible proliferative arrest, altered chromatin organization, apoptosis resistance, tumor suppressor activation, and increased protein synthesis.[17–21] Cellular senescence can be induced by conditions such as nuclear DNA damage, oxidative stress, and telomere dysfunction [22]. Cdkn2a/p16^{Ink4a} and Cdkn1a/p21^{Cip1} have been identified as genetic markers for cellular senescence, reflecting the status of cell growth, DNA synthesis, and mitosis[23–26]. Senescence associated β-Galactosidase (SA-β-Gal), a senescence-related genetic marker, and chromosomal characteristics are commonly used to identify the senescent state in cell cultures. However, expression of these markers can vary significantly across different cell and tissue types and may exhibit sex-associated differences [27–30] .

Osteocyte mechanobiology is fundamentally linked to cytoskeletal mechanics and morphology, which are essential for maintaining bone health and function. Alterations in cell mechanics and morphology are not exclusively indicative of senescence but can signal various cellular states or responses. In this study, we specifically probe these changes in the context of exposure to pro-senescence stressors (*e.g.*, irradiation) in bone cells. By examining these alterations when cells face such stressors, we aim to establish a novel set of biophysical fingerprints that uniquely characterize cellular senescence within the bone microenvironment. We specifically explore the effects of local SASP accumulation over time on these markers, as well as the paracrine influences of SASP factors through conditioned medium (CM) experiments. By supplying CM to non-irradiated osteocyte cultures, both immediately and after generating a mature healthy culture, we aim to mimic the exposure of non-senescent cells to a SASP-rich environment and investigate their responses. Our findings highlight alterations in cytoskeletal architecture and mechanics correlated to the local and paracrine effects of pro-senescence stressors, which potentially could reflect key osteocyte mechanobiological functions. This approach not only enhances our

understanding of the direct and indirect effects of SASP factors but also provides insight into the aging process of bone through the lens of osteocyte biophysical changes.

2. Methods

2.1 Cell culture and *in vitro* senescence induction

To focus on senescence-associated changes in osteocyte biophysical properties, we employed immortalized osteocytes, specifically MLO-Y4 cells. This approach mitigated the variabilities introduced by heterogeneous primary bone cell cultures. Osteocytes were cultured following established protocols [31]. Briefly, cells were passaged twice before being plated at a density of 2×10^4 cells/35-mm^2 well. The bottom of the well plates was coated with rat tail collagen type I (0.5 mg/mL, Sigma-Aldrich) and filter-sterilized 0.02 M acetic acid (diluted from glacial, ReagentPlus®, ≥99%, Sigma-Aldrich). The growth media consisted of α-Minimum Essential Medium Eagle (αMEM, Sigma-Aldrich), supplemented with 5% fetal bovine serum (FBS, Gibco), 5% calf serum (CS, Sigma-Aldrich) [32,33], and 1% penicillin-streptomycin (P/S, 10,000 U/mL, Gibco). Half of the medium volume was replenished every four days. The cells were incubated at 37°C in a 5% CO_2 humidified chamber at confluency of less than 70% to minimize disturbance of cell morphology.

Senescence was induced *in vitro* by a single dose of 10 Gy irradiation (CellRad, Precision X-Ray, *Inc*.). Post-irradiation, cells were assessed for biophysical and biomolecular properties on days 7, 14, and 20 (irradiated study groups: D7, D14, and D20). Non-irradiated cells continuously cultured in fresh media served as the Control group (Ctrl).

2.2 CM-supplemented groups

To investigate the paracrine effect of SASP factors on healthy osteocytes, CM were collected from irradiated group after 20 days of culture and then centrifuged to collect the supernatant. Two CM groups were established: in the immediate CM group (CM-i), non-irradiated osteocytes were supplemented with CM on Day 0 of culture, while in the delayed CM group (CM-d), cells were incubated in fresh growth media for 48 hours before CM supplementation. Both CM groups were cultured for 72 days before their biophysical and biomolecular properties were assessed.

For the CM-i group, cells designated for imaging and nanoindentation were plated at a density of 1×10^5 cells/35-mm^2 well, and those for RT-qPCR were plated at 6×10^5 cells/35-mm^2 well.

In the CM-d group, osteocytes for imaging and nanoindentation were plated at the same cell density as those in the Control and Irradiated groups. Cells for RT-qPCR were also plated at 6 $\times 10^5$ cells/35-mm^2 well.

2.3 Single-cell nanoindentation

Single-cell micromechanical testing was performed on 50 random osteocytes across two wells using our new optical fiber-based interferometry nanoindenter (Pavone, Optics11 Life). Osteocytes were indented with a probe having a 3 μm radius, which is significantly smaller than their surface areas, and with a stiffness of 0.019 N/m. The nanoindentation was performed at a controlled speed of 30 μm/s, reaching a peak load of 0.01 μN, after which the probe retracted at the same speed. The mechanical properties of osteocyte cytoskeleton, characterized by Young's modulus, were analyzed using Hertzian contact mechanics [34,35]. Indentation curve fitting was conducted using DataViewer V2.5.2 (Optic11 Life) over the linear region on the loading curve, accepting $R^2 > 0.90$.

2.4 Gene expression

Gene expression analysis was conducted according to the manufacturer's protocols. RNA was initially extracted from the cells using TRIzol (Invitrogen) followed by purification with the GeneJET RNA Purification Kit (Thermo Fisher Scientific). The concentration of RNA was measured using a NanoDrop Microvolume Spectrophotometer (Thermo Fisher Scientific). Subsequently, cDNA was synthesized from the purified RNA after genomic DNA (gDNA) digestion, using SuperScript™ IV VILO™ Master Mix with ezDNase (Invitrogen). Real-time quantitative Polymerase Chain Reaction (RT-qPCR) was performed using PowerTrack™ SYBR Green Master Mix (Applied Biosystems) with the specific forward and reverse primers listed in **Supplementary Table S1**. The RT-qPCR reactions were conducted on a Quantstudio 6 Pro system (Applied Biosystems). Gene expression results were normalized to Gapdh as the housekeeping gene using the Comparative Ct ($2^{-\Delta\Delta Ct}$) method.

2.5 SA-β-Gal staining

Following the manufacturer's protocol, cells were fixed and stained with SA-β-Gal (Cell Signaling Technology). After staining, the cells were incubated at 37°C overnight. Cells displaying a blue color were considered to be SA-β-Gal positive. Images were captured using a brightfield

microscope equipped with an Olympus XC30 camera, taking five random fields of view per well. The SA-β-Gal activity was quantified by counting the number of positive cells and normalizing this count to the total number of cells observed in each micrograph.

2.6 Immunofluorescent (IF) staining

Following the manufacturer's protocol, cells were fixed in 4% paraformaldehyde (PFA) and stained with Cellmask Orange Actin Tracking Stain (Invitrogen) to visualize filamentous actin (F-actin). The nuclei were counterstained with 4',6-diamidino-2-phenylindole (DAPI, Invitrogen). Fluorescent images were captured at seven fields of view using an inverted fluorescent microscope (Optics11 Life) equipped with a Nikon 20x objective. Imaging utilized the TRITC and DAPI channels at 545/570 nm and 350/465 nm (excitation/emission wavelengths), respectively. ImageJ 2.14.0 was used for postprocessing. The morphologies of nuclei, F-actin, and dendrites were analyzed and quantified using Cellprofiler 4.2.6 and NeuriteQuant [36], respectively. The multinucleation phenomena within the cell cultures were quantified by counting the number of multinucleated cells and normalizing over the total number of cells in each micrograph.

2.7 Statistical analysis

Statistical analyses were performed using GraphPad Prism 10. Both one-way and two-way analysis of variance (ANOVA) with Tukey's multiple comparison tests were employed, each at a 95% confidence interval. One-way ANOVA with Tukey's multiple comparison tests was utilized for the statistical analysis of SA-β-Gal activity, Young's moduli, and morphological quantifications. For the RT-qPCR data analyzing gene expression, either One-way or Two-way ANOVA with Tukey's multiple comparison tests was applied, depending on the experimental design. Statistical significance was considered to be $p < 0.05$.

3. Results and Discussion

3.1.1 Irradiated osteocytes exhibited time-dependent changes in biomolecular markers

After irradiation, SA-β-Gal positivity in osteocytes increased over time, which was visualized by increase in cytoplasmic blue staining. The SA-β-Gal-active osteocytes reached close to 100% of the population on Day 20 post-irradiation ($p < 0.0001$, **Figure 1A**), confirming successful induction of senescence phenotype by low dose irradiation in these cells.

Gene expression of senescence markers, SASP factors, and osteocyte markers were measured for all samples. $p16^{Ink4a}$ is a senescence marker that is responsible for regulating the G1/S phase of the cell cycle [37], while $p21^{Cip1}$ is another senescence marker involved in inhibiting both the G1/S and G2/M phase [38,39]. In the irradiated groups, levels of both p16 and p21 gradually increased over time, with a significant increase in p21 observed on Day 20 ($p < 0.05$; see **Figure 1B**). These findings indicate disruptions of the cell cycle in irradiated osteocytes, which as typical for senescent cells.

The inflammatory response in osteocytes can be reflected by expression levels of interleukin-6 (Il-6) and tumor necrosis factor (Tnf). The cytokine Il-6 is a SASP factor that not only stimulates osteoclast differentiation and regulates immune responses but also modulates inflammation. Expression of Il-6 increased significantly over time in the irradiated groups compared to controls ($p < 0.01$, **Figure 1C**), suggesting an escalated inflammatory response in irradiated osteocytes. This increase in Il-6 has been previously associated with compromised mechanotransduction in osteocytes [40], linking its accumulation with progressively impaired cellular function [41]. Similarly, expression of Tnf increased in the irradiated groups, which could potentially signify an increase in receptor activator of nuclear factor κB ligand (Rankl) production and suppression of osteoprotegerin (Opg) [42,43], potentially contributing to bone loss [44]. The elevated expression of both SASP factors in the irradiated groups indicates an increased inflammatory response through autocrine or paracrine effects. The particularly notable time-dependent accumulation of Il-6 underscores its critical role in the senescence-related progression of bone aging.

The ability for osteocytes to regulate bone remodeling was assessed by measuring the levels of matrix metalloproteinase (Mmp12) and bone gamma-carboxyglutamate protein (Bglap).

Mmp12, a SASP factor known for its role in ECM degradation, is critical in bone remodeling processes. Its increased activity is associated with accelerated bone resorption and potentially dysfunctional bone remodeling [45]. Expression of Mmp12 was elevated in the Irradiated groups over time, with more than a 20-fold increase by Day 20 compared to the Control ($p < 0.001$, **Figure 1C**). This result suggests intensified ECM degradation and possible remodeling dysfunction in these groups. Bglap, or osteocalcin, plays a key role in regulating bone mineralization [46]. In MLO-Y4 osteocytes, prominent expression of Bglap indicates its potential involvement in metabolic processes related to bone remodeling. The Irradiated groups had increased levels of Bglap compared to the Control group ($p < 0.0001$ for Day 7 and 14, $p < 0.001$ for Day 20, **Figure 1D**), potentially enhancing contributing to bone resorption and overall bone loss.

Gap junction protein alpha 1 (Gja1) expression can be linked to osteocyte dendrite function in terms of intercellular communication [47]. Disruption in Gja1 production has been previously associated with age-related osteoclastogenesis and bone loss [48]. A decline of Gja1 in the Irradiated groups (0.468 and 0.671-fold for Day 7 and Day 14, **Figure 1D**) suggests the reduction in cell communication function that is typical of aging cells. Interestingly, despite the increased accumulation of SASP factors (**Figure 1C**), at Days 14 and 20 there was an increase in Gja1 expression compared to Day 7. This elevation in Gja1 expression, which related to cellular survival and bone remodeling regulation, may indicate that the osteocytes exposed to higher levels of SASP factors on Days 14 and 20 triggered more intensive mechanisms to resist apoptosis. Overall, the decreased secretion of Gja1 from non-senescent levels among the irradiated groups suggests compromised dendriticities and potential bone loss.

The gene expression results evaluated by RT-qPCR suggested that over time, the irradiated group exhibited an increase in senescence markers and higher levels of pro-inflammatory cytokines. The increased expression of Bglap and the reduced expression of Gja1 further underscored declines in osteocyte mechanobiological function and potential dysregulation of bone resorption.

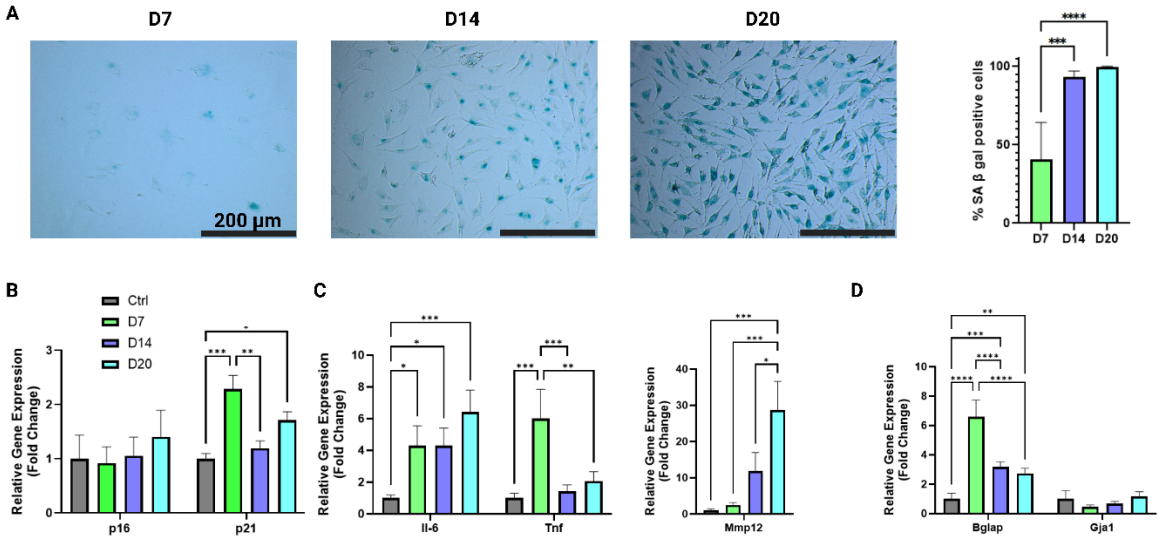

Figure 1: Time-dependent alterations in biomolecular markers among irradiated osteocytes due to local accumulation of SASP factors. A) Representative images of SA-β-Gal staining at various time points for irradiated cells (left) with quantification of SA-β-Gal active osteocytes (right). Five images per group were analyzed (n = 5). **B)** RT-qPCR results for senescence, **C)** SASP factors, and **D)** osteocyte markers at all time points. Results are normalized to GAPDH housekeeping gene expression and compared to the Control group. Sample size for each group is n = 3, presented as mean ± SD. *: $p < 0.05$, **: $p < 0.01$, ***: $p < 0.001$, ****: $p < 0.0001$.

3.1.2 Short-term SASP factor exposure induced biomolecular marker changes in healthy osteocytes

Gene expression levels from Day 7 served as the control in order to compare the local and paracrine effects of SASP factors. In the CM-i group, SASP factors were comparable to those observed on Day 7, whereas the CM-d group exhibited a 1.381-fold increase, surpassing the levels noted on Day 14. Conversely, Tnf levels in both the CM-i and CM-d groups remained low, aligning more closely with the values seen on Days 14 and 20 rather than Day 7. Mmp12 levels in both CM-supplemented groups showed a notable increase compared to Day 7 (6.239-fold and 4.047-fold, respectively; see **Figure 2C**). These results suggest that Il-6 and Mmp12 were more involved in autocrine/paracrine signaling than Tnf in the non-irradiated cells within the CM-supplemented groups. Additionally, the incubation of osteocytes in fresh growth media before supplementation with CM in the CM-d group may have stimulated a more effective uptake and signaling response

to Il-6, further amplifying its expression. Overall, these findings confirm that healthy osteocytes in both CM-supplemented groups effectively absorbed SASP factors from their conditioned media.

Expression of p16 in CM-i group was similar to that observed on Day 7, while expression in the CM-d group was lower (0.529-fold). Conversely, p21 expression increased in the CM-d group (1.509-fold), with levels in the CM-i group matching those on Day 7 (see **Figure 2B**). The stable p16 expression in the CM-i group, compared to the irradiated groups, suggests a disruption in the S phase of the cell cycle, indicating that DNA synthesis in osteocytes exposed to CM-i was significantly impacted by SASP factor exposure. On the other hand, the increase in p21 levels in the CM-d group suggests potential dysfunction in mitosis, reflecting disruption in the M phase of the cell cycle.

Bglap levels in both CM-supplemented groups were significantly lower than those observed on Day 7 ($p < 0.05$, **Figure 2D**), suggesting the paracrine effects of SASP factors were less effective in promoting osteocalcin production compared to their local effects. However, the Bglap levels in the CM-d group matched those of Day 14 (see **Figure S5**), underscoring the potential role of fresh medium incubation in stimulating healthy osteocytes. Similarly, Gja1 levels in both CM-supplemented groups showed an increase from Day 7, with levels in the CM-d group remaining similar to Day 14, whereas CM-i exhibited a significant increase compared to Day 7 ($p < 0.0001$, **Figure 2D**). This increase might be attributed to the abrupt exposure of osteocytes in the CM-i group to SASP factors in the CM triggering a more intensive survival response.

Overall, the gene expression results for the CM-supplemented osteocytes confirm effective uptake of SASP factors and suggest potential stimulation of autocrine/paracrine SASP signaling pathways. The distinctly different profiles of senescence and osteocyte markers reflect potential variations in the mechanisms through which paracrine SASP factor exposure influences non-irradiated osteocytes.

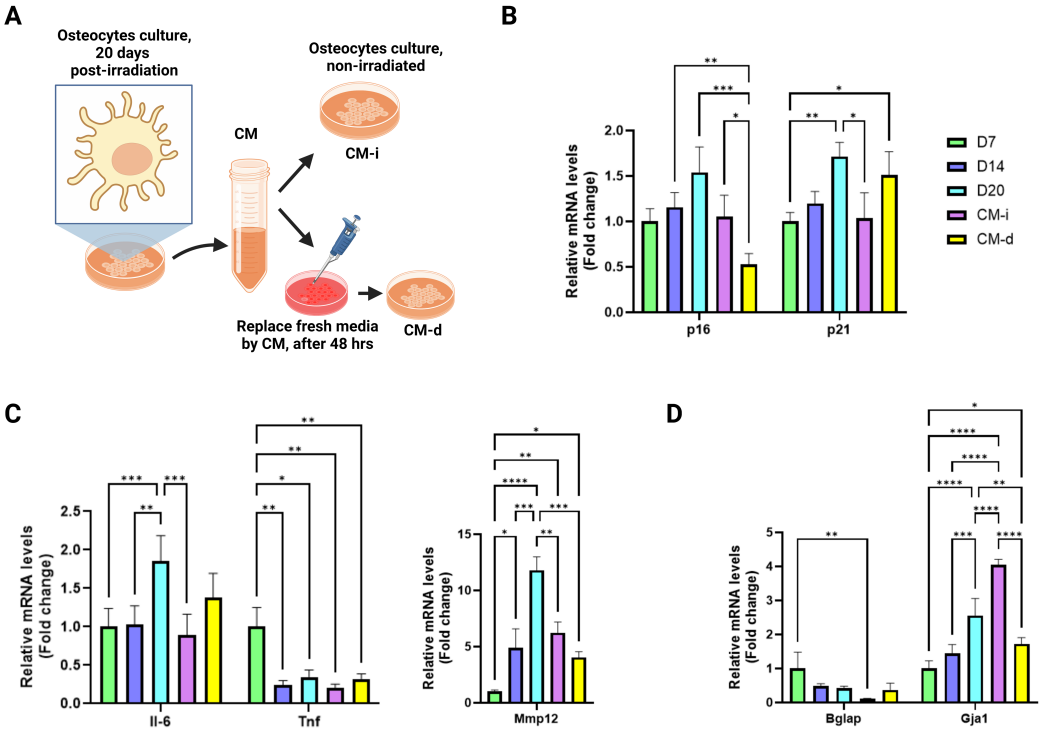

Figure 2: Paracrine exposure to SASP factors via CM-supplementation induces senescence phenotypes in healthy osteocytes. A) Schematic of the CM-i (immediate supplementation) and CM-d (delayed supplementation) culture setups. **B)** RT-qPCR results for senescence, **C)** SASP factors, and **D)** osteocyte markers across all conditions, normalized to GAPDH housekeeping gene expression and compared to the Day 7 post-irradiation group. Sample size for each group is n = 3, presented as mean ± SD. *: $p < 0.05$, **: $p < 0.01$, ***: $p < 0.001$, ****: $p < 0.0001$.

3.2 Osteocyte morphological changes as biophysical markers for senescence

Various morphological parameters were quantified in our longitudinal study to examine senescence-associated changes (**Figure 3A**). Nuclear blebbing, observed in the irradiated groups (**Figure 3B**), indicated nuclear membrane instability. Additionally, nuclear expansion was noted over time, being particularly significant on Days 14 ($p < 0.0001$) and 20 ($p < 0.001$, **Figure 3C**). In contrast, osteocytes in both CM-supplemented groups exhibited no significant changes from the control group, suggesting that short-term exposure to SASP factors may not induce profound alterations in nuclear morphology. Such stability might be attributed to mechanisms such as chromosome unwinding within the nuclei, which potentially help mitigate aging-related DNA damage. The nuclear abnormalities observed in the irradiated groups signify compromised nuclear function in osteocytes, which could lead to phenotypic variations during protein translation as

previously observed in other cell types [49,50]. These findings should be further investigated in future studies.

A significantly elevated population of multinucleated osteocytes was observed in the Irradiated groups, reaching as high as 11% on Day 20 ($p < 0.0001$, **Figure 3A, 3D**). In contrast, both CM-supplemented groups maintained similarly low levels of multinucleated cells to the Control group. Since senescent osteocytes often exhibit disrupted cell cycles, the observed multinucleation may result from incomplete M phases and/or DNA hyper-replication, similar to findings reported in oncogene-induced senescence studies of primary human fibroblasts [51]. This hypothesis is supported by the increased expression of p21 over time in the Irradiated groups, underscoring the progression of cell cycle disruption. The prevalence of multinucleation in irradiated osteocytes further emphasizes the impact of their local SASP factor accumulation, which appears to be more consequential than short-term SASP exposure from their microenvironment.

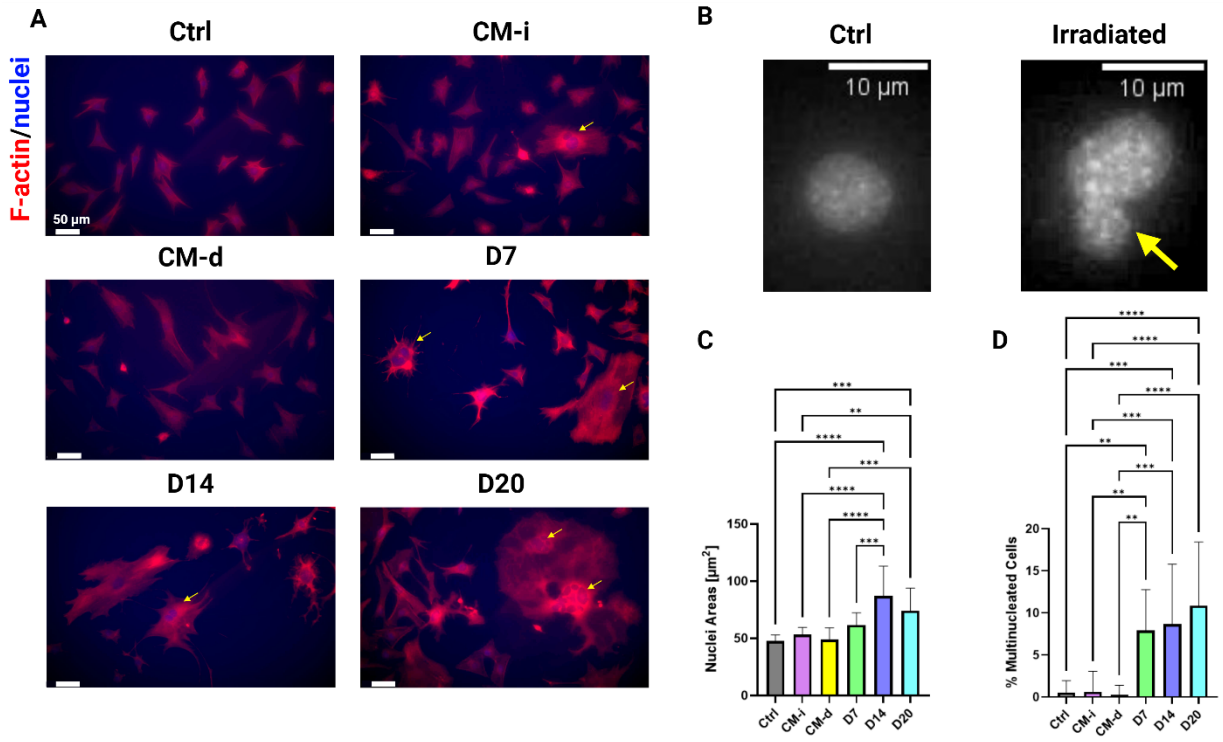

Figure 3: F-actin and nuclei morphology alterations correlated with local and paracrine SASP factor exposure. A) Representative IF micrographs showing F-actin and nuclei staining across all experimental conditions, with yellow arrows highlighting multinucleated cells. Scale bar: 50 µm. **B)** Close-up view of nuclear blebbing in irradiated osteocytes, indicated by a yellow arrow. **C)** Average nuclear areas quantified using CellProfiler from IF micrographs across all conditions. **D)** Percentages of multinucleated osteocytes in each experimental group.

Quantitative analysis of osteocyte morphology was performed by examining 14 IF micrographs per group across two cell culture wells (n = 14 for all groups, presented as mean ± SD). Significance levels are denoted as *: $p < 0.05$, **: $p < 0.01$, ***: $p < 0.001$, ****: $p < 0.0001$.

F-actin networks in osteocytes from the Irradiated groups exhibited extensive expansion compared to the Control group, characterized by reduced dendricity and non-uniform organization of F-actin structures (**Figures 3A**, **4A**). This alteration was likely due to oxidative stress induced by irradiation, which may have led to actin disassembly in the osteocytes [52]. A progressive time-dependent increase in the average F-actin area was observed in the Irradiated groups ($p < 0.0001$), significantly exceeding that of the Control and both CM-supplemented groups (**Figure 4B**). This increase could be attributed to abnormal filopodia and lamellipodia formation in senescent cells, which likely contributed to osteocyte flattening and area expansion. The disorganized and expanded F-actin networks may have resulted in spatially heterogeneous mechanical properties within the osteocytes. These findings demonstrate that local SASP factor accumulation significantly altered osteocyte F-actin morphology, potentially impairing their mechanobiological function. In contrast, the paracrine effects of SASP factors were less pronounced in influencing F-actin expansion, likely due to the relatively brief exposure to oxidative stress compared to the longer-term exposure experienced by osteocytes in the Irradiated groups.

The dendrite lengths of irradiated osteocytes were observed to be generally shorter compared to the Control group (see **Figure S3**). Furthermore, both CM-supplemented groups exhibited a declining trend in dendrite length relative to the Control (see **Figure S3**). To mitigate confounding effects due to variations in F-actin area, dendrite lengths were normalized to soma areas. This analysis revealed that normalized dendrite lengths in the Irradiated group significantly decreased by Day 14 ($p < 0.0001$) and continued to decline through Day 20 ($p < 0.001$, **Figure 4D**). The dendritic lengths in both CM-supplemented groups were also reduced compared to the Control cells, aligning with measurements from Day 7, suggesting compromised osteocyte structure due to paracrine SASP factor exposure.

We also observed that Gja1 levels were consistent with compromised dendritic morphology across all conditions when compared to the Control (see **Figure 1E**), further supporting the hypothesis that reduced dendritic lengths serve as a relevant and prominent biophysical marker of osteocyte senescence correlated with SASP factor local and paracrine accumulation. These results

indicate that irradiated and CM-supplemented osteocytes, on average, exhibit diminished dendritic network connectivity, which may suggest reduced intercellular communication and mechanosensation capabilities. This diminished connectivity is indicative of substantial alterations in osteocyte mechanobiological function.

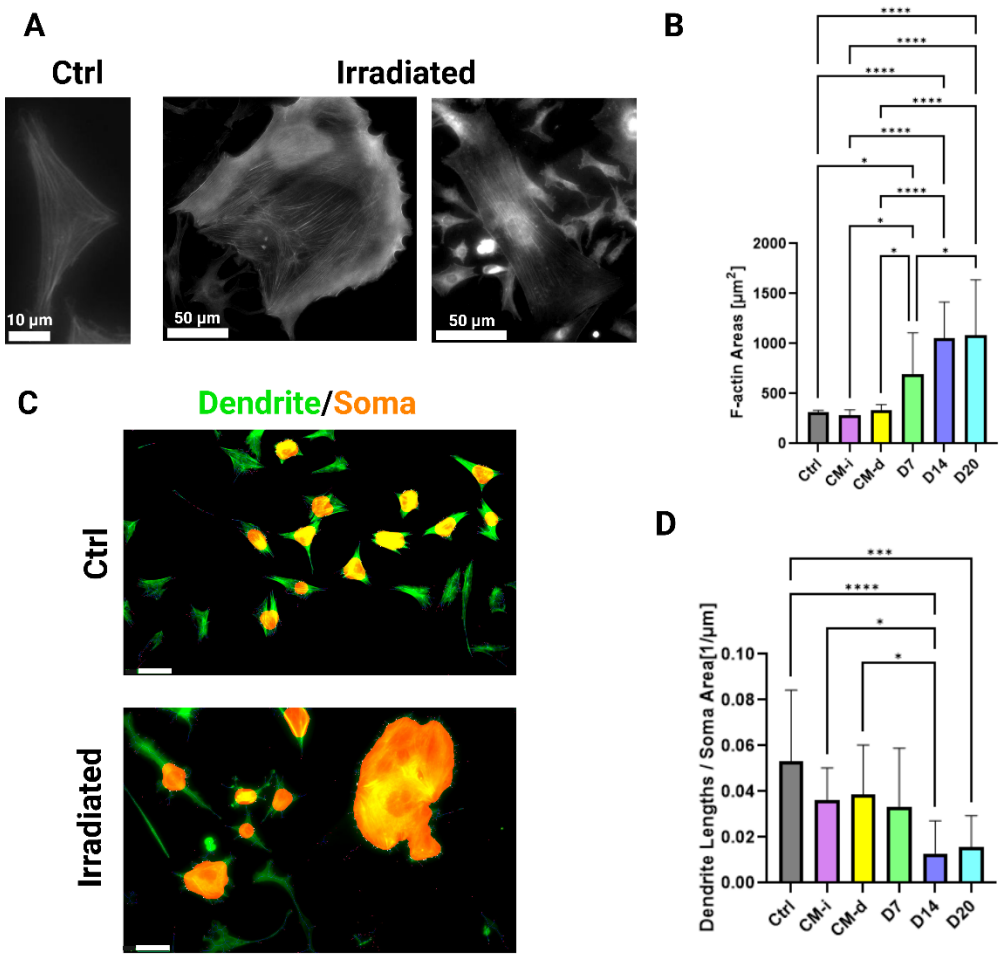

Figure 4: Deviations in F-actin areas and dendricities in osteocytes exposed to SASP factors compared to non-senescent cells. A) Representative images of F-actin organization in osteocytes from Control and Irradiated groups. Scale bar: Control: 10 µm, Irradiated: 50 µm. **B)** Quantification of average F-actin areas using CellProfiler from IF micrographs across all experimental conditions. **C)** Representative images of semi-automated segmentation and quantification of dendrites and soma performed using NeuriteQuant. Scale bar: 50 µm. **D)** Quantification of average dendrite length normalized to soma area, calculated from IF micrographs of all conditions using NeuriteQuant. All quantitative osteocyte morphology results were obtained by analyzing 14 IF micrographs per group across two cell culture wells (n = 14 for all groups, presented as mean ± SD). Significance levels are indicated as *: $p < 0.05$, **: $p < 0.01$, ***: $p < 0.001$, ****: $p < 0.0001$.

3.3 Osteocyte cytoskeleton stiffening as a biophysical marker for senescence

To characterize the longitudinal changes in cytoskeletal stiffness due to local and paracrine exposure to SASP factors, we employed live single-cell nanoindentation (**Figures 5A-B**). At all study time points, osteocytes from the Irradiated groups exhibited significantly higher Young's modulus (*i.e*. stiffnesses) compared to those in the Control and CM-supplemented groups (see **Figure 5C**). Notably, the CM-d group displayed a trend toward increased stiffness compared to the Control, which may highlight the role of cell maturation prior to CM-supplementation in enhancing the uptake of SASP factors by osteocytes (**Figure 5C**). This increase in cytoskeletal moduli could be linked to the previously demonstrated expansion in F-actin area (see **Figure 4B**).

The stiffening of the osteocyte cytoskeleton, coupled with the observed senescence-associated heterogeneity in cytoskeletal organization (**Figure 4A**), suggests a decline in cell motility and possibly mechanosensory properties. Such degenerative changes potentially lead to deterioration in interactions of osteocytes with the ECM, a phenomenon similarly reported in studies involving fibroblasts [53]. These findings indicate that while irradiated osteocytes consistently exhibit cytoskeletal stiffening, paracrine exposure to SASP factors results in less significant change in cytoskeletal stiffness.

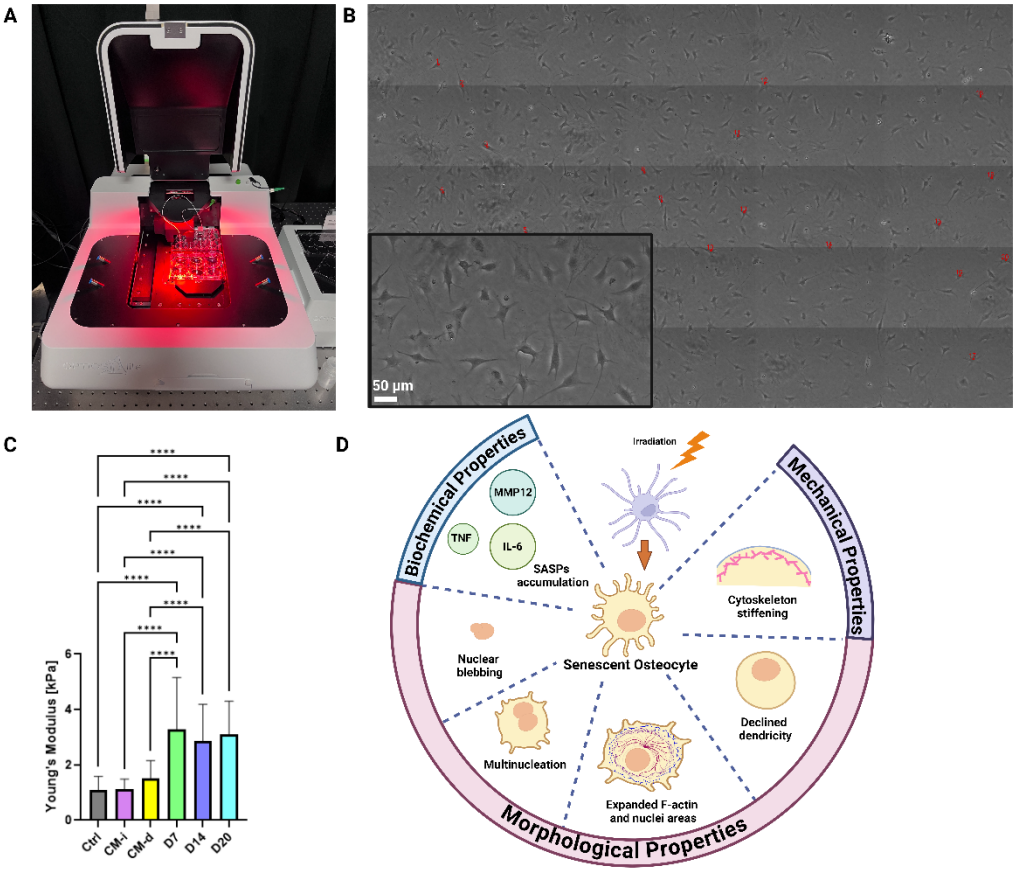

Figure 5: Significant cytoskeletal stiffening in irradiated osteocytes. A) Representative image of our live single-cell mechanical testing setup. **B)** Live cells attached to the bottom of the cell culture plate being indented. Red dots indicate the probe size and locations of indentation. **C)** Young's moduli of osteocytes cytoskeleton measured using Hertzian contact mechanic model. Data from 50 cells per condition are presented as mean ± SD. Significance levels are denoted as *: $p < 0.05$, **: $p < 0.01$, ***: $p < 0.001$, ****: $p < 0.0001$. **D)** Summary of the study: Irradiation-induced senescence in osteocytes is characterized by changes in micromechanical properties, morphological features, and biomolecular markers.

4. Conclusions and Future Directions

This longitudinal study has elucidated the impact of continuous local SASP factor accumulation as a result of irradiation on distinct senescence-associated biophysical markers, corroborated by corresponding biomolecular markers. Our findings underscore how changes in cytoskeletal architecture and mechanics are intricately linked to osteocyte senescence. Moreover, experimental observations at various time points revealed nuclear morphological changes characteristic of senescence, which were supported by gene expression profiles related to senescence, SASP factors, and osteocyte markers. This reinforces the consistency between genomic and biophysical markers in depicting a time-dependent deterioration in cytoskeletal structure and mechanics.

While significant paracrine effects of SASP factors on expression of senescence biomarkers were observed, the CM groups demonstrated no substantial changes in biophysical properties, particularly cytoskeletal Young's modulus or morphological properties, when compared to the healthy control group. This indicates that the local accumulation of SASP factors has a more pronounced impact on the biophysical properties of healthy osteocytes.

Our study's reliance on a 2D *in vitro* culture system presents inherent limitations. Although useful for controlled studies, such models do not fully capture the complex three-dimensional architecture and mechanical dynamics of bone tissue, potentially restricting the direct applicability of these findings to *in vivo* contexts. Furthermore, 2D cultures may not entirely capture the intercellular interactions and extracellular matrix dynamics found in living tissues, which are crucial for cellular behavior and function. The inclusion of proteomic measures in future studies could enhance the characterization of SASP factors and offer a more comprehensive understanding of senescence processes.

Moving forward, we recommend the adoption of 3D culture systems or organ-on-a-chip models to more accurately emulate the bone microenvironment. This approach, coupled with validating physiologically relevant *in vitro* models using longitudinal studies in transgenic mouse models, could provide deeper insights into bone remodeling dynamics and the roles of senescence markers *in vivo*. These methods will not only help validate our findings but also potentially unveil additional mechanisms and therapeutic targets for combating bone diseases associated with aging.

Author Contributions

MT designed the study, experiments, and concept. JL and MT performed the experiments, researched, analyzed, interpreted the data, and wrote the original manuscript. MT, JLK, and KMM provided resources. All authors reviewed and revised the manuscript. All authors read and approved the final manuscript.

Acknowledgements

This research and MT are supported by the Walker Department of Mechanical Engineering at The University of Texas at Austin. KMM is supported by NCI (RO1 CA198279 and CA250905).

Conflict of Interest Statement

The authors declare no conflict of interest in regard to this work.

Data Availability

The data that support the findings of this study are available on request from the corresponding author.

References

[1] N. Sarafrazi, *Osteoporosis or Low Bone Mass in Older Adults: United States, 2017-2018*, Atlanta, Georgia, **2021**.

[2] U. Herbig, M. Ferreira, L. Condel, D. Carey, J. M. Sedivy, *Science (1979)* **2006**, *311*, 1257.

[3] F. Wang, F. Cai, R. Shi, X.-H. Wang, X.-T. Wu, *Osteoarthritis Cartilage* **2016**, *24*, 398.

[4] R. J. Pignolo, S. F. Law, A. Chandra, *JBMR Plus* **2021**, *5*, DOI 10.1002/jbm4.10488.

[5] S. Chaib, T. Tchkonia, J. L. Kirkland, *Nat Med* **2022**, *28*, 1556.

[6] J. N. Farr, M. Xu, M. M. Weivoda, D. G. Monroe, D. G. Fraser, J. L. Onken, B. A. Negley, J. G. Sfeir, M. B. Ogrodnik, C. M. Hachfeld, N. K. LeBrasseur, M. T. Drake, R. J. Pignolo, T. Pirtskhalava, T. Tchkonia, M. J. Oursler, J. L. Kirkland, S. Khosla, *Nature Medicine 2017 23:9* **2017**, *23*, 1072.

[7] S. Chaib, T. Tchkonia, J. L. Kirkland, *Nat Med* **2022**, *28*, 1556.

[8] U. Tripathi, A. Misra, T. Tchkonia, J. L. Kirkland, *Mech Ageing Dev* **2021**, *198*, 111548.

[9] S. Lopes-Paciencia, E. Saint-Germain, M.-C. Rowell, A. F. Ruiz, P. Kalegari, G. Ferbeyre, *Cytokine* **2019**, *117*, 15.

[10] S. Khosla, J. N. Farr, J. L. Kirkland, *J Clin Endocrinol Metab* **2018**, *103*, 1282.

[11] J. N. Farr, S. Khosla, *Bone* **2019**, *121*, 121.

[12] A. M. D. Malone, N. N. Batra, G. Shivaram, R. Y. Kwon, L. You, C. H. Kim, J. Rodriguez, K. Jair, C. R. Jacobs, *American Journal of Physiology-Cell Physiology* **2007**, *292*, C1830.

[13] W. M. Jackson, M. J. Jaasma, R. Y. Tang, T. M. Keaveny, *American Journal of Physiology-Cell Physiology* **2008**, *295*, C1007.

[14] Q. Wan, E. Cho, H. Yokota, S. Na, *J Bone Miner Metab* **2013**, *31*, 520.

[15] N. B. M. Rafiq, Y. Nishimura, S. V. Plotnikov, V. Thiagarajan, Z. Zhang, S. Shi, M. Natarajan, V. Viasnoff, P. Kanchanawong, G. E. Jones, A. D. Bershadsky, *Nat Mater* **2019**, *18*, 638.

[16] S. Seetharaman, S. Etienne-Manneville, *J Cell Sci* **2019**, *132*, DOI 10.1242/jcs.232843.

[17] T. Tchkonia, Y. Zhu, J. Van Deursen, J. Campisi, J. L. Kirkland, *J Clin Invest* **2013**, *123*, DOI 10.1172/JCI64098.

[18] N. A. Sims, *Journal of Bone and Mineral Research* **2016**, *31*, 1917.

[19] J. N. Farr, S. Khosla, *Bone* **2019**, *121*, 121.

[20] J. N. Farr, J. Kaur, M. L. Doolittle, S. Khosla, J. Farr, M. Doolittle, *Curr Osteoporos Rep* **2020**, *18*, 559.

[21] S. Khosla, J. N. Farr, T. Tchkonia, J. L. Kirkland, *Nat Rev Endocrinol* **2020**, *16*, 263.

[22] A. Hernandez-Segura, J. Nehme, M. Demaria, *Trends Cell Biol* **2018**, *28*, 436.

[23] D. A. Alcorta, Y. Xiong, D. Phelps, G. Hannon, D. Beach, J. C. Barrett, *Proceedings of the National Academy of Sciences* **1996**, *93*, 13742.

[24] M. Fischer, M. Quaas, L. Steiner, K. Engeland, *Nucleic Acids Res* **2016**, *44*, 164.

[25] A. O. Masson, R. Hess, K. O'Brien, K. L. Bertram, P. Tailor, E. Irvine, G. Ren, R. J. Krawetz, *Mech Ageing Dev* **2015**, *149*, 31.

[26] X. CHEN, W. ZHANG, Y. F. GAO, X. Q. SU, Z. H. ZHAI, *Cell Res* **2002**, *12*, 229.

[27] M. J. Yousefzadeh, J. Zhao, C. Bukata, E. A. Wade, S. J. McGowan, L. A. Angelini, M. P. Bank, A. U. Gurkar, C. A. McGuckian, M. F. Calubag, J. I. Kato, C. E. Burd, P. D. Robbins, L. J. Niedernhofer, *Aging Cell* **2020**, *19*, DOI 10.1111/acel.13094.

[28] M. Rall-Scharpf, T. W. P. Friedl, S. Biechonski, M. Denkinger, M. Milyavsky, L. Wiesmüller, *Aging* **2021**, *13*, 21066.

[29] B. Wang, L. Wang, N. S. Gasek, C. L. Kuo, J. Nie, T. Kim, P. Yan, J. Zhu, B. L. Torrance, Y. Zhou, L. C. Flores, C. Allen, A. M. Andrade, C. Guo, R. L. Cohn, E. R. Jellison, J. M. Bartley, G. A. Kuchel, S. Li, T. Pirtskhalava, T. Tchkonia, S. Yadav, L. Haynes, J. L. Kirkland, Y. Ikeno, M. Xu, *Cell Metab* **2024**, *36*, 1795.

[30] M. Ogrodnik, J. Carlos Acosta, P. D. Adams, F. d'Adda di Fagagna, D. J. Baker, C. L. Bishop, T. Chandra, M. Collado, J. Gil, V. Gorgoulis, F. Gruber, E. Hara, P. Jansen-Dürr, D. Jurk, S. Khosla, J. L. Kirkland, V. Krizhanovsky, T. Minamino, L. J. Niedernhofer, J. F. Passos, N. A. R. Ring, H. Redl, P. D. Robbins, F. Rodier, K. Scharffetter-Kochanek, J. M. Sedivy, E. Sikora, K. Witwer, T. von Zglinicki, M. H. Yun, J. Grillari, M. Demaria, *Cell* **2024**, *187*, 4150.

[31] Y. Kato, J. J. Windle, B. A. Koop, G. R. Mundy, L. F. Bonewald, *Journal of Bone and Mineral Research* **1997**, *12*, 2014.

[32] B. Zhang, P. Shang, *STAR Protoc* **2024**, *5*, 103186.

[33] S. L. York, P. Sethu, M. M. Saunders, *Ann Biomed Eng* **2016**, *44*, 1170.

[34] C. A. Grant, D. J. Brockwell, S. E. Radford, N. H. Thomson, *Biophys J* **2009**, *97*, 2985.

[35] A. Demichelis, C. Divieto, L. Mortati, S. Pavarelli, G. Sassi, M. P. Sassi, *J Biomech* **2015**, *48*, 1099.

[36] L. Dehmelt, G. Poplawski, E. Hwang, S. Halpain, *BMC Neurosci* **2011**, *12*, 100.

[37] D. A. Alcorta, Y. Xiong, D. Phelps, G. Hannon, D. Beach, J. C. Barrett, *Proceedings of the National Academy of Sciences* **1996**, *93*, 13742.

[38] A. B. Niculescu, X. Chen, M. Smeets, L. Hengst, C. Prives, S. I. Reed, *Mol Cell Biol* **1998**, *18*, 629.

[39] T. Ando, T. Kawabe, H. Ohara, B. Ducommun, M. Itoh, T. Okamoto, *Journal of Biological Chemistry* **2001**, *276*, 42971.

[40] J. D. Gardinier, A. Chougule, C. Zhang, *J Cell Physiol* **2022**, *237*, 2249.

[41] L. Qin, W. Liu, H. Cao, G. Xiao, *Bone Res* **2020**, *8*, 23.

[42] B. F. Boyce, L. Xing, *Arch Biochem Biophys* **2008**, *473*, 139.

[43] M. C. Walsh, Y. Choi, *Front Immunol* **2014**, *5*, DOI 10.3389/fimmu.2014.00511.

[44] G. Schett, S. Hayer, J. Zwerina, K. Redlich, J. S. Smolen, *Nat Clin Pract Rheumatol* **2005**, *1*, 47.

[45] S. M. Krane, M. Inada, *Bone* **2008**, *43*, 7.

[46] M. H. Raymond, B. C. Schutte, J. C. Torner, T. L. Burns, M. C. Willing, *Genomics* **1999**, *60*, 210.

[47] H. M. Davis, R. Pacheco-Costa, E. G. Atkinson, L. R. Brun, A. R. Gortazar, J. Harris, M. Hiasa, S. A. Bolarinwa, T. Yoneda, M. Ivan, A. Bruzzaniti, T. Bellido, L. I. Plotkin, *Aging Cell* **2017**, *16*, 551.

[48] D. Zhao, R. Liu, G. Li, M. Chen, P. Shang, H. Yang, J. X. Jiang, H. Xu, *Front Physiol* **2020**, *11*, DOI 10.3389/fphys.2020.00299.

[49] A. Buchwalter, M. W. Hetzer, *Nat Commun* **2017**, *8*, 328.

[50] I. Heckenbach, G. V. Mkrtchyan, M. Ben Ezra, D. Bakula, J. S. Madsen, M. H. Nielsen, D. Oró, B. Osborne, A. J. Covarrubias, M. L. Idda, M. Gorospe, L. Mortensen, E. Verdin, R. Westendorp, M. Scheibye-Knudsen, *Nat Aging* **2022**, *2*, 742.

[51] D. Dikovskaya, J. J. Cole, S. M. Mason, C. Nixon, S. A. Karim, L. McGarry, W. Clark, R. N. Hewitt, M. A. Sammons, J. Zhu, D. Athineos, J. D. G. Leach, F. Marchesi, J. van Tuyn,

S. W. Tait, C. Brock, J. P. Morton, H. Wu, S. L. Berger, K. Blyth, P. D. Adams, *Cell Rep* **2015**, *12*, 1483.

[52] A. Milzani, I. DalleDonne, R. Colombo, *Arch Biochem Biophys* **1997**, *339*, 267.

[53] C. Schulze, F. Wetzel, T. Kueper, A. Malsen, G. Muhr, S. Jaspers, T. Blatt, K.-P. Wittern, H. Wenck, J. A. Käs, *Biophys J* **2010**, *99*, 2434.